frontiers in Materials

ORIGINAL RESEARCH
published: 04 March 2022
doi: 10.3389/fmats.2022.826795

Optical Properties and Dynamic Extrinsic Chirality of Structured Monolayer Black Phosphorus

Mengke Sun, Ying Wang, Hui Hu, Hao Zhang, Wenjia Li, Bo Lv, Zheng Zhu, Chunying Guan and Jinhui Shi**

College of Physics and Optoelectronic Engineering, Harbin Engineering University, Harbin, China

Chiral metamaterials have drawn increasing attention due to their strong chiral responses. Monolayer black phosphorus is a tunable two-dimensional material with anisotropy that plays an important role in a variety of fields such as chirality and polarization control. In this work, we propose a metamaterial with structured monolayer black phosphorus to manipulate the transmission properties of circularly polarized waves. The metamaterial exhibits strong circular dichroism and circular birefringence effects depending on oblique incidence of the circularly polarized wave and has a weaker circular conversion dichroism effect as well. Moreover, this work also investigates effects of different chiral phenomena of the metamaterial on various structural parameters as well as incident angles and the electron concentration. It has been proved that the electron concentration of monolayer black phosphorus can dynamically tune the chirality properties. Remarkably, the non-zero pure optical activity always occurs at one certain frequency regardless of the elevation angle and the azimuthal angle. The proposed framework provides opportunities for designing meta-devices with monolayer black phosphorus and practical potentials for novel and high-performance infrared metamaterials.

Keywords: metamaterial, black phosphorus, extrinsic chirality, circular dichroism (CD), circular birefringence

OPEN ACCESS

Edited by:
Wei-Xiang Jiang,
Southeast University, China

Reviewed by:
Tun Cao,
Dalian University of Technology, China
Zuojia Wang,
Zhejiang University, China

****Correspondence:***
Wenjia Li
liwenjia@hrbeu.edu.cn
Jinhui Shi
shijinhui@hrbeu.edu.cn

Specialty section:
This article was submitted to Metamaterials, a section of the journal Frontiers in Materials

Received: *01 December 2021*
Accepted: *20 January 2022*
Published: *04 March 2022*

Citation:
Sun M, Wang Y, Hu H, Zhang H, Li W, Lv B, Zhu Z, Guan C and Shi J (2022) Optical Properties and Dynamic Extrinsic Chirality of Structured Monolayer Black Phosphorus. Front. Mater. 9:826795. doi: 10.3389/fmats.2022.826795

INTRODUCTION

In the past years, many attempts have been made to realize the manipulation for phase, amplitude, and polarization of electromagnetic waves by exploiting metamaterials (Shi et al., 2014; Gansel et al., 2015; Scheuer, 2017; Yang et al., 2018). Metamaterials, a kind of artificial structures, can be elaborately designed to acquire extraordinary and unique properties including negative refraction, perfect lens, giant chiral response, and nonlinearity (Shelby et al., 2001). Metamaterials can be also extended into diverse fields, such as electromagnetism, acoustics, and mechanics (Deng et al., 2019; Fan et al., 2019; Thevamaran et al., 2019). Chiral objects lack mirror symmetry, and it cannot superimpose with its mirror image through planar translation or rotation. Chirality plays an indispensable role in chemistry, biology, and medicines (Lewis et al., 1999; Čorić and List, 2012; Collins et al., 2017). However, since chiralities of natural materials are inherently limited, metamaterials with giant chiral responses have attracted considerable attention and shown importance in optics (Rogacheva et al., 2006; Decker et al., 2010; Zhou et al., 2012). Chirality has been classified into intrinsic chirality and extrinsic chirality. Extrinsic chirality refers to chiral response of achiral anisotropic planar metamaterials at oblique incidence (Plum et al., 2009a; Plum et al., 2009b). To achieve extrinsic chirality, two-dimensional (2D) materials, including graphene and black phosphorus (BP), have drawn

much attention over the past decade (Shi et al., 2018; Wei et al., 2020) because they have excellent electromagnetic and optical properties. With the comprehensive study of 2D materials, BP has gradually become one of the most popular materials for its unique optical properties including intrinsic anisotropy and has been explored for extensive applications such as polarization converters (Valagiannopoulos et al., 2017; Cheng et al., 2019) and plasmonic devices (Liu and Aydin, 2016; Hong et al., 2018).

Different from other 2D materials (Chen et al., 2019), BP is the most stable allotrope of phosphorus with a stratified structure that breaks narrow bandgap limitation and low absorption efficiency of graphene. In addition, BP has tunable thickness-dependent bandgaps changing from 0.35 eV (bulk) to 2 eV (monolayer), filling up the "blank space" between graphene and transition-metal dichalcogenides (Li et al., 2014; Chen et al., 2015; Saito and Iwasa, 2015; Jia et al., 2020). Thus, BP has been widely studied and applied in some electronic devices, such as field effect transistors (Buscema et al., 2014a; Liu et al., 2014; Wang et al., 2014; Liu et al., 2016), photovoltaic devices (Buscema et al., 2014b), rechargeable batteries (Park and Sohn, 2007), solar cells (Zhou et al., 2016), and heterostructures (Shen et al., 2015; Niu et al., 2019). On the other hand, BP has a large tunable bandgap. Thus, the manipulation of electromagnetic waves with BP, such as absorbers (Lu et al., 2015; Niu et al., 2018; Kong et al., 2019) and reconfigurable color display (Jia et al., 2021), has aroused widespread interest. The monolayer BP is composed of hexagonal honeycomb lattice with a folded structure (Low et al., 2014; Hong et al., 2019). Due to strong in-plane anisotropy, BP is one of the most important 2D materials to manipulate the polarization state of light as well as polarization-dependent optical phenomena. At mid-infrared wavelength, polarization-dependent localized surface plasmon resonances have been studied and numerically verified in monolayer BP nanoribbon and nanopatch arrays (Liu and Aydin, 2016). The optical activity resulting from the extrinsic chirality has been proved theoretically and numerically in unpatterned monolayer BP, which can be adjusted by the mutual orientation of the in-plane anisotropic BP film and the incident light (Hong et al., 2019). The monolayer BP is promising to realize tunable polarization manipulation; however, chiral metamaterials with the whole BP layer have limited tunable properties and working frequency range.

In this work, we propose monolayer nanostructured BP metamaterial, patterned on a dielectric substrate and study its optical properties, such as transmittance, optical activity, and circular conversion dichroism. In addition, the dependence of optical properties in the BP metamaterial is presented on different parameters including the period, duty ratio, doping concentration levels of the monolayer BP, and angle of incidence. The different parameters differently impact the chiral responses; thus, nanostructured square BP is beneficial to realize diverse optical properties. Compared with the previously reported monolayer BP (Hong et al., 2019), the designed monolayer BP metamaterial has more flexibilities and more freedoms to tailor tunable circular response. The proposed structure is promising to design various novel and high-performance infrared metamaterials.

DESIGN AND ANALYSIS OF THE TUNABLE METAMATERIAL

The proposed structure is schematically illustrated in **Figure 1A**. The armchair and zigzag directions of the monolayer BP are along *x*- and *y*-directions, respectively. The square BP marked by the black box is periodically patterned on a dielectric substrate with a relative dielectric constant of 4 and relative permeability of 1. Both periodicities along *x* and *y* directions are identical and marked by *p*. The doping concentration level of the monolayer BP is denoted as *n*. The BP thickness is assumed to be 1 nm, and the width is *w*. The parameter *w* is equal to the product of the period (*p*) and the duty ratio (*k*). The angle between the wave vector and the *z*-direction is defined as the elevation angle β, and the angle between the incidence plane and the *x*-direction is defined as the azimuthal angle α. The metamaterial will exhibit chiral response at oblique incidence of the circularly polarized wave. A frequency domain solver is adopted, and the periodic boundary conditions are applied along *x* and *y* directions in software Microwave Studio (CST).

To demonstrate the extrinsic chirality of the designed metamaterial, the electromagnetic responses of the square BP are simulated as shown from **Figure 1B** to **Figure 1E**, in which $n = 6 \times 10^{13}$ cm^{-2}, $p = 500$ nm, $k = 0.95$, $\beta = 75^{\circ}$, and $\alpha = 45^{\circ}$. The circular dichroism (labeled as Δ) can be written by

$$\Delta = T_{++} - T_{--}, \tag{1}$$

where the subscripts "+" and "–" denote right-handed circularly polarized light (RCP) and left-handed circularly polarized light (LCP), respectively, and the order of the subscripts corresponds to transmission and incidence, respectively. The transmittance is expressed as $T_{ij} = |t_{ij}|^2$, where *t* represents the magnitude of electromagnetic waves and "*i*" as well as "*j*" represents the transmitted and incident electric components, respectively. The circular birefringence (labeled as Φ) and circular conversion dichroism (labeled as δ) can be given by

$$\Phi = \arg(t_{++}) - \arg(t_{--}); \tag{2}$$

$$\delta = T_{-+} - T_{+-}. \tag{3}$$

It is obvious in **Figure 1B** that the square BP metamaterial distinctly responses to the incident RCP and LCP waves in the nearly whole wavelength range. Both the transmittance spectra T_{++} and T_{--} exhibit resonant dips at the wavelength ranging between 20–30 μm. The transmittance T_{++} and T_{--} are different except for the cross point at about 26 μm; thus, the square BP metamaterial reveals extrinsic chirality at oblique incidence since it is intrinsically achiral. The relatively weak circular polarization conversion is shown in **Figure 1B**. The co-polarization transmittance is several times higher than the cross-polarization transmittance. Similar to the co-polarization transmittance spectra, there is a cross point between two cross-polarization transmittance spectra at about 26 μm, and they are different somewhere else. The circular dichroism of the

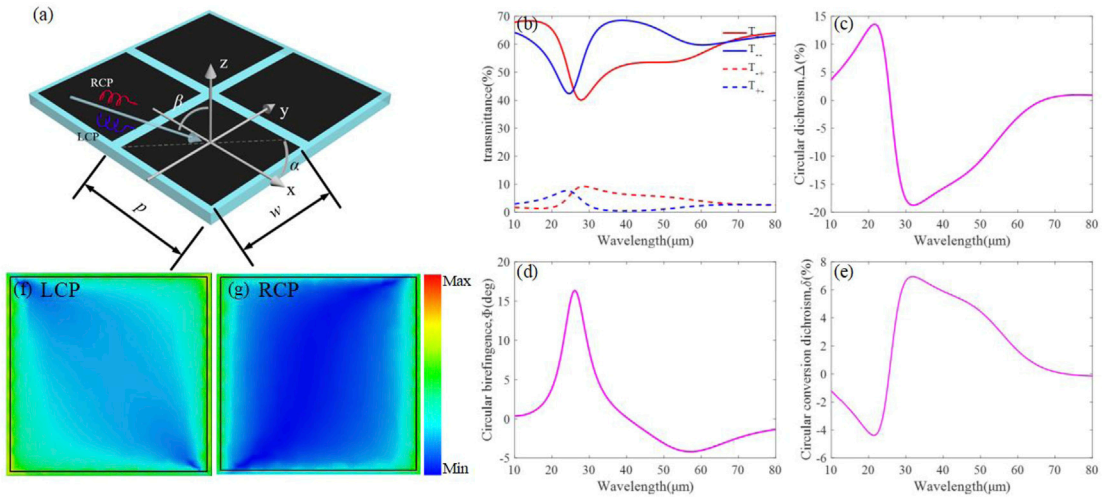

FIGURE 1 | (A) Illustration of the square monolayer BP metamaterial. The metamaterial consists of an array of square BP nanostructures. The red and blue arrows indicate right-handed (RCP) and left-handed (LCP) circularly polarized waves, respectively. α denotes the azimuthal angle between the incident plane and the *x*-direction. β denotes the elevation angle. **(B)** Transmittance, **(C)** circular dichroism, **(D)** circular birefringence, and **(E)** circular conversion dichroism of the square BP metamaterial. Here, $n = 6 \times 10^{13}$ cm^{-2}, $p = 500$ nm, $k = 0.95$, $\beta = 75^{\circ}$, and $\alpha = 45^{\circ}$. The EM field distribution of the BP metamaterial for the **(F)** LCP and **(G)** RCP incidence.

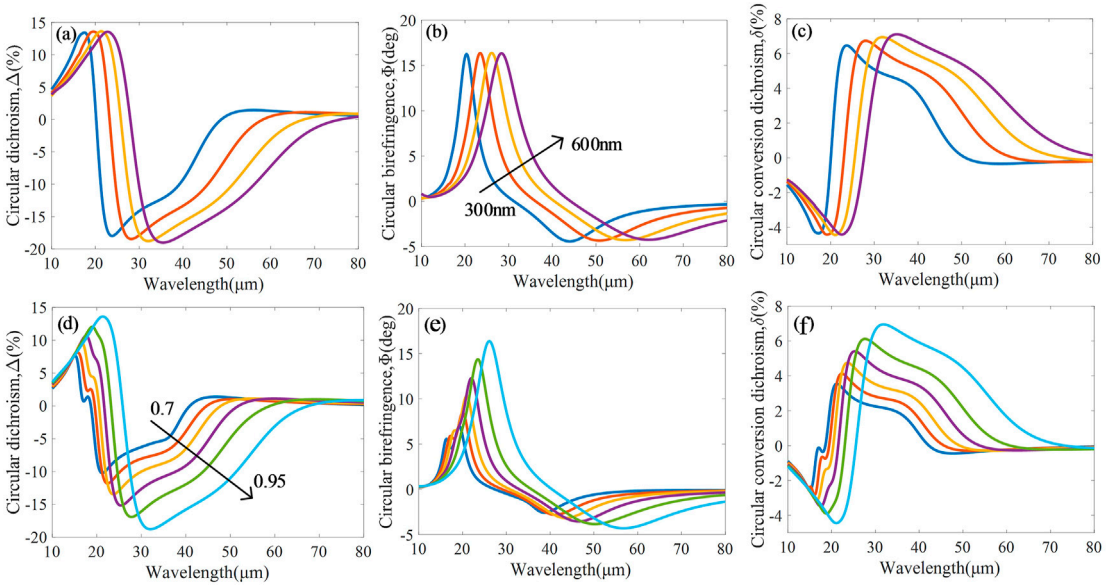

FIGURE 2 | Dependences of **(A)** circular dichroism, **(B)** circular birefringence, and **(C)** circular conversion dichroism on the period of the square BP metamaterial with $k = 0.95$, $n = 6 \times 10^{13}$ cm^{-2}, $\beta = 75^{\circ}$, and $\alpha = 45^{\circ}$. Dependences of **(D)** circular dichroism, **(E)** circular birefringence, and **(F)** circular conversion dichroism on the duty ratio of the square BP metamaterial with $p = 500$ nm, $n = 6 \times 10^{13}$ cm^{-2}, $\beta = 75^{\circ}$, and $\alpha = 45^{\circ}$.

metamaterial is shown in **Figure 1C**. The signs of the two circular dichroism peaks are opposite due to the respective resonances of two circularly polarized waves. The peak value is 14.0% at the wavelength of 21.3 μm, indicating that the RCP transmittance is greater than that of LCP. Moreover, the peak value of the circular dichroism is −18.8% at the wavelength of 32.3 μm, indicating that the LCP transmittance is higher. **Figure 1D** shows that the maximum circular birefringence is 16.4° at the wavelength of ~26.1 μm, while the circular dichroism is 0 at the wavelength of ~26 μm; as a result, the metamaterial exhibits a pure optical activity, and the transmitted wave is linearly polarized. **Figure 1E** displays the circular conversion dichroism. The circular conversion dichroism is up to 7% at the wavelength of ~30 μm that is twice as large as that in the reported metamaterial with a whole BP layer (Hong et al., 2019). **Figures 1F,G** depict the field patterns of the proposed metamaterial with the LCP and RCP incidence, respectively, which is used to tell the optical difference between

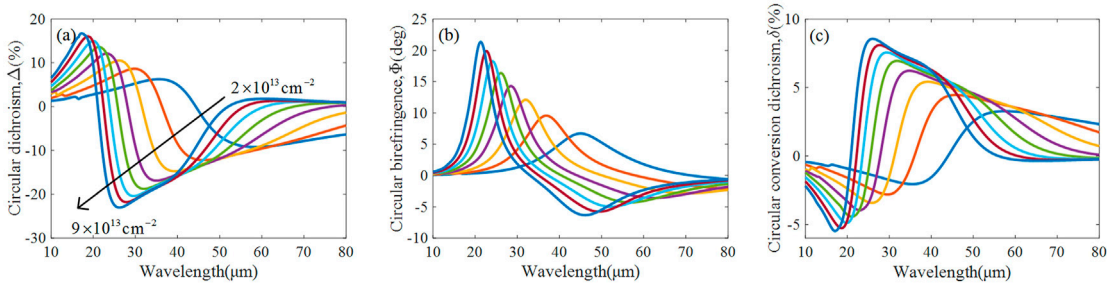

FIGURE 3 | Influences of the doping concentration level on the chiral responses of the square BP metamaterial. The doping concentration level changes from 2 × 10^{13} cm^{-2} to 9 × 10^{13} cm^{-2} with a step of 1 × 10^{13} cm^{-2}. **(A)** Circular dichroism Δ, **(B)** circular birefringence Φ, and **(C)** circular conversion dichroism δ.

LCP and RCP waves (Cao et al., 2013; Cao et al., 2015; Cao et al., 2017). The circular conversion dichroism spectrum of the designed BP structure varies a lot with the wavelength. Compared to the previous literature (Hong et al., 2019), the square BP metamaterial offers versatile chiral responses and abundant resonances for easily tailoring the polarization properties.

To fully explore multiple parameters-tailored chiral responses, we investigate how the responses of the square BP metamaterial depend on various structural parameters including period, duty ratio, doping concentration level, and angle of incidence. The conditions of $n = 6 \times 10^{13}$ cm^{-2}, $\beta = 75^{\circ}$, and $\alpha = 45^{\circ}$ are kept unchanged in **Figure 2**. The effects of the period and the duty ratio on the chiral responses are studied. **Figures 2A–C** show the dependence of the circular dichroism, circular birefringence, and circular conversion dichroism on the period ranging from 300 to 600 nm at an interval of 100 nm, in which $k = 0.95$. In fact, the period and the width of the square BP scale up or down together due to a fixed duty ratio. The peak values of all the responses remain unchanged with different periods, while the corresponding resonant wavelengths largely have red shifts with the increasing period. During the period change, the resonant wavelengths shift more than 30% (the shift is larger than 10 μm). The chiral responses can be well engineered *via* parameter study.

Next, the dependences of the circular dichroism, the circular birefringence, and the circular conversion dichroism are investigated on the duty ratio shown in **Figures 2D–F**. The duty ratio changes from 0.7 to 0.95 with a step of 0.05 while $p = 500$ nm, $n = 6 \times 10^{13}$ cm^{-2}, $\beta = 75^{\circ}$, and $\alpha = 45^{\circ}$ remain constant. The effect of the duty ratio is quite different from the aforementioned one. With the increase of the duty ratio in the range of 0.7–0.95, the peak values of all the chiral responses increase, and all the spectra move toward longer wavelengths. On the other hand, in **Figures 2A–F**, the tendency of the curves is alike with different duty ratios. Thus, the positions and amplitudes of the resonant peaks are changed simultaneously with different duty ratios. The resonances of the circular dichroism, circular birefringence, and circular conversion dichroism of the metamaterial could be moved to the required wavelength by changing the period and the duty ratio.

To well understand tunable chiral responses of the square BP metamaterial, it is necessary to study the effect of the doping concentration level of monolayer BP. **Figures 3A–C** depict the changes of circular dichroism, circular birefringence, and circular conversion dichroism with different doping concentration levels. The doping concentration level varies from 2 × 10^{13} cm^{-2} to 9 × 10^{13} cm^{-2} with a step of 1 × 10^{13} cm^{-2} while $p = 500$ nm, $k = 0.95$, $\beta = 75^{\circ}$, and $\alpha = 45^{\circ}$ are kept unchanged. The two resonant values of the circular dichroism spectrum vary from 6.2 to 16.7% and from −9.2% to −23%, respectively. The corresponding wavelengths alter from 36 to 17.4 μm and from 57.5 to 26 μm, respectively. **Figure 3A** implies that the metamaterial has a giant extrinsic chirality and reveals tunability in a broad frequency range. With the increase of the doping concentration level, the resonant peaks of the circular birefringence spectrum increase and the resonant wavelengths have a large blue shift. When the doping concentration level is 2 × 10^{13} cm^{-2}, the metamaterial has a weak chirality effect, while the maximum value of the circular birefringence can reach 21.3° as the doping concentration level is 9 × 10^{13} cm^{-2}. In addition, the circular conversion dichroism becomes stronger when the doping concentration level increases. The tuning ranges of three chiral responses are as high as 50%, for instance, the resonance of the circular dichroism spectrum moves from 36 to 17.4 μm. Therefore, the tunable extrinsic chirality of the BP metamaterial is strongly related to the doping concentration level. The doping concentration level is one of the most important parameters to actively modulate the chiral response of the metamaterial. In the proposed metamaterial, the chirality could be controlled by the doping concentration level of the square BP *via* the electric field, pressure, temperature, and light, especially it can act as a switch in the wavelength from 20 to 30 μm, which can modulate the chirality of the metamaterial by changing the doping concentration level of monolayer BP. Obviously, the structure can be optimized before the metamaterial is manufactured just by choosing appropriate parameters including period. Moreover, when the metamaterial is designed, BP as a tunable material can also achieve dynamic optical phenomena such as the increase or decrease of chiral properties through various doping concentration levels instead of redesigning the structure.

For the proposed structure, there is no chirality for the incident circularly polarized wave at normal incidence. It is necessary to study the angular dependence of the extrinsic chiral responses in the square BP metamaterial, while all other geometrical and physical parameters are unchanged as those in **Figures 1B–E**. The angular dependences of the metamaterial's responses are shown in **Figure 4** when the elevation angle β and the azimuthal angle α are individually

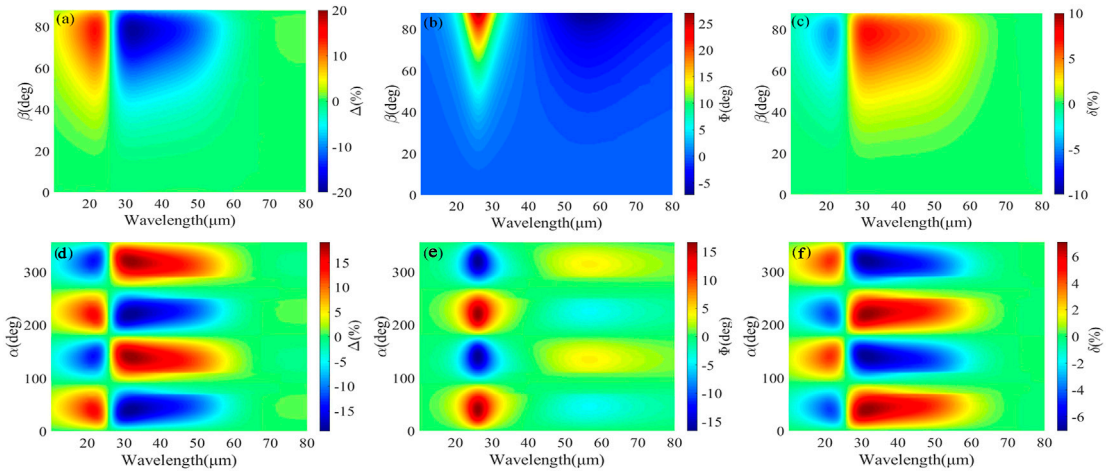

FIGURE 4 | Dependences of **(A)** circular dichroism Δ, **(B)** circular birefringence Φ, and **(C)** circular conversion dichroism δ on the elevation angle β. Here, $\alpha = 45^{\circ}$. Dependences of **(D)** circular dichroism Δ, **(E)** circular birefringence Φ, and **(F)** circular conversion dichroism δ on the azimuthal angle α. Here, $\beta = 75^{\circ}$.

changed. All circular dichroism, circular birefringence, and circular conversion dichroism are mostly dictated by the elevation angle β in **Figures 4A–C**, in which $\alpha = 45^{\circ}$. When β is small, the metamaterial does not exhibit any chiral responses including circular dichroism, circular birefringence, and circular conversion dichroism due to the symmetry of the metamaterial. With increasing β, the extrinsic chirality occurs, and the chiral responses manifest their maxima at large angle of incidence. The circular dichroism, circular birefringence, and circular conversion dichroism reach their maxima of −18.8%, 28°, and 7%, respectively. Remarkably, the non-zero pure optical activity phenomenon always occurs at ~26 μm regardless of the elevation angle β. It can be seen from **Figures 4A–C** that there is a significant characteristic in the vicinity of the wavelength 26 μm, in which the circular dichroism and the circular conversion dichroism are opposite at the left and right sides of this wavelength, and the circular birefringence always reach its resonance. Here, $\beta = 75^{\circ}$. The chiral properties of the square BP metamaterial are shown in **Figure 4D**–**Figure 4F** when the azimuthal angle α varies in the full range of 360°. All spectra are periodically produced at every 180°, and their signs are reversed at every 90°. When the azimuthal angle α is 0°, 90°, 180°, and 270°, the whole system combined with the proposed structure and the incident circularly polarized waves is symmetric; thus, the chirality vanishes in the square BP metamaterial. The pure optical activity at 26 μm does not shift with the azimuthal angle. Thus, the incident angles α and β provide a way to engineer the extrinsic chirality in the square BP metamaterial.

CONCLUSION

In conclusion, we have proposed a metamaterial with monolayer BP patches to demonstrate a giant tunability of the extrinsic chirality. The circular dichroism, circular birefringence, and circular conversion dichroism of the metamaterial have been numerically investigated. The extrinsic chirality can be well engineered to work in a broad frequency range via studying the parameters such as period, duty ratio, doping concentration level, and angle of incidence. The circular conversion dichroism is up to 7% at the wavelength of ~30 μm, which is twice as large as that in the whole BP layer. The doping concentration level of the square BP metamaterial leads to large tuning ranges of three chiral responses up to 50%. Remarkably, the non-zero pure optical activity always occurs at one certain frequency regardless of the elevation angle and the azimuthal angle, and the circular birefringence reaches 28°. Compared to the whole BP layer in the previous literatures, the square BP metamaterial offers versatile chiral responses and abundant resonances for easily tailoring the polarization properties. The proposed metamaterial with BP patches is promising to realize active polarization manipulation as well as chiral switching and biological chiral sensing.

DATA AVAILABILITY STATEMENT

The raw data supporting the conclusion of this article will be made available by the authors, without undue reservation.

AUTHOR CONTRIBUTIONS

MS, YW, and HH contributed to the conception and design of the study. MS performed the design simulation and wrote the first draft of the manuscript. YW and HH performed the statistical analysis. YW, WL, and JS wrote the sections of the manuscript. WL and JS supervised the project. All authors contributed to manuscript revision and read, and approved the submitted version.

FUNDING

This work was supported in part by the National Natural Science Foundation of China under Grant No. 62175049, in part by the

Natural Science Foundation of Heilongjiang Province in China under Grant No. ZD 2020F002, in part by the 111 Project to the Harbin Engineering University under Grant No. B13015, and in part by the Fundamental Research Funds for the Central Universities under Grant Nos. 3072021CFT2501 and 3072021CF2505.

REFERENCES

Buscema, M., Groenendijk, D. J., Steele, G. A., van der Zant, H. S., and Castellanos-Gomez, A. (2014). Photovoltaic Effect in Few-Layer Black Phosphorus PN Junctions Defined by Local Electrostatic Gating. *Nat. Commun.* 5 (1), 4651–4656. doi:10.1038/ncomms5651

Buscema, M., Groenendijk, D. J., Blanter, S. I., Steele, G. A., van der Zant, H. S. J., and Castellanos-Gomez, A. (2014). Fast and Broadband Photoresponse of Few-Layer Black Phosphorus Field-Effect Transistors. *Nano Lett.* 14 (6), 3347–3352. doi:10.1021/nl5008085

Cao, T., Li, Y., Wei, C.-W., and Qiu, Y.-m. (2017). Numerical Study of Tunable Enhanced Chirality in Multilayer Stack Achiral Phase-Change Metamaterials. *Opt. Express* 25 (9), 9911–9925. doi:10.1364/oe.25.009911

Cao, T., Wei, C.-W., Mao, L.-B., and Wang, S. (2015). Tuning of Giant 2D-Chiroptical Response Using Achiral Metasurface Integrated with Graphene. *Opt. Express* 23 (14), 18620–18629. doi:10.1364/oe.23.018620

Cao, T., Zhang, L., Simpson, R. E., Wei, C., and Cryan, M. J. (2013). Strongly Tunable Circular Dichroism in Gammadion Chiral Phase-Change Metamaterials. *Opt. Express* 21 (23), 27841–27851. doi:10.1364/oe.21.027841

Chen, G., Lin, X., and Wang, Z. (2019). Enhanced Reflective Dichroism from Periodic Graphene Ribbons via Total Internal Reflection. *Opt. Express* 27 (16), 22508–22521. doi:10.1364/oe.27.022508

Chen, Y., Jiang, G., Chen, S., Guo, Z., Yu, X., Zhao, C., et al. (2015). Mechanically Exfoliated Black Phosphorus as a New Saturable Absorber for Both Q-Switching and Mode-Locking Laser Operation. *Opt. Express* 23 (10), 12823–12833. doi:10.1364/oe.23.012823

Cheng, Y., Li, W., and Mao, X. (2019). Triple-band Polarization Angle Independent 90° Polarization Rotator Based on Fermat's Spiral Structure Planar Chiral Metamaterial. *Pier* 165, 35–45. doi:10.2528/pier18112603

Collins, J. T., Kuppe, C., Hooper, D. C., Sibilia, C., Centini, M., and Valev, V. K. (2017). Chirality and Chiroptical Effects in Metal Nanostructures: Fundamentals and Current Trends. *Adv. Opt. Mater.* 5 (16), 1700182. doi:10.1002/adom.201700182

Čorić, I., and List, B. (2012). Asymmetric Spiroacetalization Catalysed by Confined Brønsted Acids. *Nature* 483 (7389), 315–319. doi:10.1038/nature10932

Decker, M., Zhao, R., Soukoulis, C. M., Linden, S., and Wegener, M. (2010). Twisted Split-Ring-Resonator Photonic Metamaterial with Huge Optical Activity. *Opt. Lett.* 35 (10), 1593–1595. doi:10.1364/ol.35.001593

Deng, B., Tournat, V., Wang, P., and Bertoldi, K. (2019). Anomalous Collisions of Elastic Vector Solitons in Mechanical Metamaterials. *Phys. Rev. Lett.* 122 (4), 44101. doi:10.1103/physrevlett.122.044101

Fan, B., Nasir, M. E., Nicholls, L. H., Zayats, A. V., and Podolskiy, V. A. (2019). Magneto - Optical Metamaterials: Nonreciprocal Transmission and Faraday Effect Enhancement. *Adv. Opt. Mater.* 7 (14), 1801420. doi:10.1002/adom.201801420

Gansel, J. K., Thiel, M., Rill, M. S., Decker, M., Bade, K., Saile, V., et al. (2015). Gold helix Photonic Metamaterial as Broadband Circular Polarizer. *Science* 325 (5947), 1513–1515. doi:10.1126/science.1177031

Hong, Q., Xu, W., Zhang, J., Zhu, Z., Yuan, X., and Qin, S. (2019). Optical Activity in Monolayer Black Phosphorus Due to Extrinsic Chirality. *Opt. Lett.* 44 (7), 1774–1777. doi:10.1364/OL.44.001774

Hong, Q., Xiong, F., Xu, W., Zhu, Z., Liu, K., Yuan, X., et al. (2018). Towards High Performance Hybrid Two-Dimensional Material Plasmonic Devices: strong and Highly Anisotropic Plasmonic Resonances in Nanostructured Graphene-Black Phosphorus Bilayer. *Opt. Express* 26 (17), 22528–22535. doi:10.1364/oe.26.022528

Jia, J. Y., Ban, Y., Liu, K., Mao, L. B., Su, Y., Lian, M., et al. (2021). Reconfigurable Full Color Display Using Anisotropic Black Phosphorus. *Adv. Opt. Mater.* 9 (16), 2100499. doi:10.1002/adom.202100499

Jia, J. Y., Chen, X. M., Ban, Y., Zhang, X. Y., Liu, K., Guo, Y. M., et al. (2020). Gap-Plasmon Induced One-Order Enhancement of Optical Anisotropy of 2D Black Phosphorus. *Adv. Photon. Res.* 1 (1), 2000010. doi:10.1002/adpr.202000010

Kong, X., Wang, Z., Du, L., Niu, C., Sun, C., Zhao, J., et al. (2019). Optically Transparent Metamirror with Broadband Chiral Absorption in the Microwave Region. *Opt. Express* 27 (26), 38029–38038. doi:10.1364/oe.383666

Lewis, D. L., Garrison, A. W., Wommack, K. E., Whittemore, A., Steudler, P., and Melillo, J. (1999). Influence of Environmental Changes on Degradation of Chiral Pollutants in Soils. *Nature* 401 (6756), 898–901. doi:10.1038/44801

Li, L., Yu, Y., Ye, G. J., Ge, Q., Ou, X., Wu, H., et al. (2014). Black Phosphorus Field-Effect Transistors. *Nat. Nanotech* 9 (5), 372–377. doi:10.1038/nnano.2014.35

Liu, F., Zhu, C., You, L., Liang, S.-J., Zheng, S., Zhou, J., et al. (2016). 2D Black Phosphorus/SrTiO3-Based Programmable Photoconductive Switch. *Adv. Mater.* 28 (35), 7768–7773. doi:10.1002/adma.201602280

Liu, H., Neal, A. T., Zhu, Z., Luo, Z., Xu, X., Tománek, D., et al. (2014). Phosphorene: an Unexplored 2D Semiconductor with a High Hole Mobility. *ACS Nano* 8 (4), 4033–4041. doi:10.1021/nn501226z

Liu, Z., and Aydin, K. (2016). Localized Surface Plasmons in Nanostructured Monolayer Black Phosphorus. *Nano Lett.* 16 (6), 3457–3462. doi:10.1021/acs.nanolett.5b05166

Low, T., Rodin, A. S., Carvalho, A., Jiang, Y. J., Wang, H., Xia, F. N., et al. (2014). Tunable Optical Properties of Multilayer Black Phosphorus Thin Films. *Phys. Rev. B* 90 (7), 075434. doi:10.1103/physrevb.90.075434

Lu, S. B., Miao, L. L., Guo, Z. N., Qi, X., Zhao, C. J., Zhang, H., et al. (2015). Broadband Nonlinear Optical Response in Multi-Layer Black Phosphorus: an Emerging Infrared and Mid-infrared Optical Material. *Opt. Express* 23 (9), 11183–11194. doi:10.1364/oe.23.011183

Niu, C. N., Wang, Z. J., Zhao, J., Du, L. G., Liu, N., Liu, Y. M., et al. (2019). Photonic Heterostructures for Spin-Flipped Beam Splitting. *Phys. Rev. Appl.* 12 (4), 044009. doi:10.1103/physrevapplied.12.044009

Niu, C., Zhao, J., Du, L., Liu, N., Wang, Z., Huang, W., et al. (2018). Spatially Dispersive Dichroism in Bianisotropic Metamirrors. *Appl. Phys. Lett.* 113 (26), 261102. doi:10.1063/1.5053794

Park, C.-M., and Sohn, H.-J. (2007). Black Phosphorus and its Composite for Lithium Rechargeable Batteries. *Adv. Mater.* 19 (18), 2465–2468. doi:10.1002/adma.200602592

Plum, E., Liu, X.-X., Fedotov, V. A., Chen, Y., Tsai, D. P., and Zheludev, N. I. (2009). Metamaterials: Optical Activity without Chirality. *Phys. Rev. Lett.* 102 (11), 113902. doi:10.1103/physrevlett.102.113902

Plum, E., Zhou, J., Dong, J., Fedotov, V. A., Koschny, T., Soukoulis, C. M., et al. (2009). Metamaterial with Negative index Due to Chirality. *Phys. Rev. B* 79 (3), 035407. doi:10.1103/physrevb.79.035407

Rogacheva, A. V., Fedotov, V. A., Schwanecke, A. S., and Zheludev, N. I. (2006). Giant Gyrotropy Due to Electromagnetic-Field Coupling in a Bilayered Chiral Structure. *Phys. Rev. Lett.* 97, 177401. doi:10.1103/PhysRevLett.97.177401

Saito, Y., and Iwasa, Y. (2015). Ambipolar Insulator-To-Metal Transition in Black Phosphorus by Ionic-Liquid Gating. *ACS Nano* 9 (3), 3192–3198. doi:10.1021/acsnano.5b00497

Scheuer, J. (2017). Metasurfaces-based Holography and Beam Shaping: Engineering the Phase Profile of Light. *Nanophotonics* 6 (1), 137–152. doi:10.1515/nanoph-2016-0109

Shelby, R. A., Smith, D. R., and Schultz, S. (2001). Experimental Verification of a Negative index of Refraction. *Science* 292 (5514), 77–79. doi:10.1126/science.1058847

Shen, Z., Sun, S., Wang, W., Liu, J., Liu, Z., and Yu, J. C. (2015). A Black-Red Phosphorus Heterostructure for Efficient Visible-Light-Driven Photocatalysis. *J. Mater. Chem. A.* 3 (7), 3285–3288. doi:10.1039/c4ta06871h

Shi, J. H., Ma, H. F., Guan, C. Y., Wang, Z. P., and Cui, T. J. (2014). Broadband Chirality and Asymmetric Transmission in Ultrathin 90°-twisted Babinet-Inverted Metasurfaces. *Phys. Rev. B* 89 (16), 165128. doi:10.1103/physrevb.89.165128

Shi, J., Li, Z., Sang, D. K., Xiang, Y., Li, J., Zhang, S., et al. (2018). THz Photonics in Two Dimensional Materials and Metamaterials: Properties, Devices and Prospects. *J. Mater. Chem. C* 6 (6), 1291–1306. doi:10.1039/c7tc05460b

Thevamaran, R., Branscomb, R. M., Makri, E., Anzel, P., Christodoulides, D., Kottos, T., et al. (2019). Asymmetric Acoustic Energy Transport in Non-

hermitian Metamaterials. *The J. Acoust. Soc. America* 146 (1), 863–872. doi:10.1121/1.5114919

Valagiannopoulos, C. A., Mattheakis, M., Shirodkar, S. N., and Kaxiras, E. (2017). Manipulating Polarized Light with a Planar Slab of Black Phosphorus. *J. Phys. Commun.* 1 (4), 045003. doi:10.1088/2399-6528/aa90c8

Wang, H., Wang, X., Xia, F., Wang, L., Jiang, H., Xia, Q., et al. (2014). Black Phosphorus Radio-Frequency Transistors. *Nano Lett.* 14 (11), 6424–6429. doi:10.1021/nl5029717

Wei, C. W., Dereshgi, S. A., Song, X. L., Murthy, A., Dravid, V. P., Cao, T., et al. (2020). Polarization Reflector/Color Filter at Visible Frequencies via Anisotropic α-MoO3. ". *Adv. Opt. Mater.* 8 (11), 2000088. doi:10.1002/adom.202000088

Yang, B., Guo, Q., Tremain, B., Liu, R., Barr, L. E., Yan, Q., et al. (2018). Ideal Weyl Points and Helicoid Surface States in Artificial Photonic crystal Structures. *Science* 359 (6379), 1013–1016. doi:10.1126/science.aaq1221

Zhou, J. F., Chowdhury, D. R., Zhao, R. K., Azad, A. K., Chen, H. T., Soukoulis, C. M., et al. (2012). Terahertz Chiral Metamaterials with Giant and Dynamically Tunable Optical Activity. *Phys. Rev. B* 86 (3), 035448. doi:10.1103/physrevb.86.035448

Zhou, L., Zhang, J., Zhuo, Z., Kou, L., Ma, W., Shao, B., et al. (2016). Novel Excitonic Solar Cells in Phosphorene-TiO2 Heterostructures with Extraordinary Charge Separation Efficiency. *J. Phys. Chem. Lett.* 7 (10), 1880–1887. doi:10.1021/acs.jpclett.6b00475

Conflict of Interest: The authors declare that the research was conducted in the absence of any commercial or financial relationships that could be construed as a potential conflict of interest.

Publisher's Note: All claims expressed in this article are solely those of the authors and do not necessarily represent those of their affiliated organizations, or those of the publisher, the editors, and the reviewers. Any product that may be evaluated in this article, or claim that may be made by its manufacturer, is not guaranteed or endorsed by the publisher.